REMOTE SPECTRAL DETECTION USING A LABORATORY SIGNATURE

A. Schaum

Naval Research Laboratory, Washington DC, USA

ABSTRACT

Two new algorithms are derived for remotely detecting a material characterized only by its laboratory spectrum. The methods are motivated by the practical difficulties in predicting an accurate field radiance from a reflectance. The first algorithm associates an affine subspace with the material, instead of a radiance point. The second algorithm is designed to prevent false alarms from dark pixels, to which the first algorithm may be sensitive. Both algorithms are ideally suited for use in conjunction with a simple method of vicarious calibration, which is also described.

Index Terms—spectrum, signature, matched filter, affine

1. BACKGROUND

The matched filter (*MF*) is a popular tool in hyperspectral remote sensing for locating objects that span several pixels. However, it is ideally suited for a different type of problem. The MF requires that: (1) uncertainty in the mean object signature be confined to a known spectral direction through the clutter mean, and (2) object and clutter covariances must agree. These conditions make the MF most suitable for the detection of extreme sub-pixel objects. Furthermore, the mean signature required in (1) must be available in radiance space, and this information is not readily available in many important applications, even if laboratory signatures are.

Here we develop an alternative *affine* matched filter (*AMF*), which is more appropriate for detecting extended targets, and which accommodates practical uncertainties in target signature knowledge. AMF is ideal when used in conjunction with another new method we describe, called *Virtual Relative Calibration* (*VRC*), for generating a radiance space representation of a laboratory reflectance signature. VRC is related to the *QUick Atmospheric Correction (QuAC)* [1] method but is much simpler.

References [2, 3] reported extremely low false alarm rate performance for the combined AMF-VRC technique, which was applied to materials with known laboratory reflectance spectra. It was noted, however, that dark pixels (shaded or with low reflectivity) consistently responded more strongly to the AMF than well-lit or highly reflective ones. For more difficult detection problems, such as targets embedded in higher clutter or with weak signatures, dark pixels could prove problematical. Therefore, the standard clutter model was extended to include dark pixels.

This enhancement expands the standard statistical model of hyperspectral clutter to accommodate variable levels of illumination. When incorporated into the affine target model, it generates another algorithm, the Joint Affine Matched Filter (*JAMF*). In field tests, JAMF substantially reduced dark pixel response with no noticeable reduction in target detectability.

Achieving better detection results than some straw man technique, for example the matched filter, is the theme of too many hyperspectral reports. The usual exercise consists of applying a new detection technique with several free parameters to a particular data set and adjusting the parameters until an optimal result can be cited. Such demonstrations of performance potential are common, but the algorithms seldom find their way into practice, unless a convincing phenomenological or theoretical basis for them can be established. Anecdotal demonstrations say nothing about the generalizability of a new algorithm to different targets or to different background clutter.

The successful demonstration in [2, 3] of AMF and JAMF is not immune to a charge of anecdotalism. The algorithms were applied to a single data set, albeit one with a large number of pixels. The aim of this paper is to complement that work with a firm theoretical foundation for the AMF and JAMF algorithms, neither of which has any adjustable parameters.

2. CLUTTER/TARGET STATISTICAL MODELS

We use the common multivariate Gaussian model for hyperspectral clutter. The standard statistical estimates of mean and covariance matrix are assumed to have been derived from the data according to

$$\mu_r = \frac{1}{N}\sum_{i=1}^{N} r_i \ , \qquad C_r = \frac{1}{N}\sum_{i=1}^{N} (r_i - \mu_r)(r_i - \mu_r)^t \ , \quad (1)$$

where r_i is a D-dimensional vector (D bands of data) representing the spectral radiance of the i^{th} of N pixels.

Based on the estimates in (1), we will carry out all calculations in "whitened" space, defined by the transformation:

$$x = C_r^{-\frac{1}{2}} r \,. \tag{2}$$

In this space, distances that naturally arise in the mathematical expression of detection algorithms are usually Euclidean, and so afford a geometrical interpretation. This view was used in [2] to motivate the algorithms, which are derived here from established principles of detection theory.

Equation (2) implies that matrices derived from radiance vectors change according to the transformation:

$$M = C_r^{-\frac{1}{2}} M_r C_r^{-\frac{1}{2}}. \tag{3}$$

For example, the covariance matrix in Equation (1) becomes the identity matrix *I*. This simplifies the Gaussian probability model for the clutter to

$$p_C(x) = \frac{1}{(2\pi)^{d/2}} \exp\left(-\frac{1}{2}(x-\mu)^2\right), \tag{4}$$

with the whitened clutter mean defined by $\mu = C_r^{-\frac{1}{2}} \mu_r$. The projection of x into any direction has unit variance for the distribution in (4), called the *core* clutter model.

We model the probability function for the target similarly as

$$p_T(x) = \frac{1}{(2\pi)^{d/2}} \exp\left(-\frac{1}{2}(x-T)^2\right), \tag{5}$$

the same as (4), but with target mean *T*. Equation (5) implies that the whitened target covariance equals that of the clutter. This implies in turn that a target's variability in radiance space is identical to that of the clutter and so is described by C_r (see Equation (1)). This may be a crude approximation, but it is motivated by sensor utility and atmospheric phenomenology in the SWIR, as explained below.

One of the principal incentives for using short-wave sensors is their long slant-range atmospheric penetrability, which is associated with the transparency of haze in the SWIR. On the other hand, long slant ranges enhance adjacency effects, in which the sensed radiance of each pixel becomes corrupted by neighboring pixels through atmospheric scattering [4]. We incorporate this effect approximately in our model of the sensing process by ascribing to a target the same covariance matrix as that of its neighboring background pixels. To further justify this assumption, we note that for most rare targets: (1) No better model of the effect of the clutter on sensed target variability is known, and (2) no information about the intrinsic target variability exists.

The only formal difference between our target and clutter model distributions is in their mean values. A good estimate of the clutter mean μ is assumed to be derivable from field measurements. If a good estimate of *T* is also available, then the best detector is known to be a likelihood ratio (LR) test: Declare a test pixel *x* a target if the ratio of (5) to (4) exceeds some predetermined threshold.

However, in our development of the AMF, *T* in Equation (5) will not represent a known mean value, unlike the μ of Equation (4). Therefore, an LR test cannot be evaluated. Instead, *T* will denote a partially unknown parameter, necessitating a so-called Generalized Likelihood Ratio (*GLR*) test to generate the detection algorithm.

3. TARGET SIGNATURE TRANSLATION

As discussed in [2], most naturally occurring background materials, except for green vegetation, have nearly graybody (flat) spectra in SWIR wavelengths. Therefore, if S_i is the solar spectrum in band *i* filtered through the atmosphere, and τ_i is the atmospheric transmissivity on the path from ground to sensor, then assuming other illumination sources and path radiances are negligible, a target radiance $(T_r)_i$ should satisfy

$$(T_r)_i \approx \tau_i S_i (\rho_T)_i \,, \tag{6}$$

where ρ_T is the target reflectivity.

Similarly, if ρ_C is the reflectivity of a clutter pixel, then we can expect the clutter ensemble to satisfy

$$(\mu_r)_i \approx \langle \tau_i S_i (\rho_C)_i \rangle \approx \tau_i S_i \langle (\rho_C)_i \rangle \propto \tau_i S_i, \tag{7}$$

where < > denotes expected value, and the final relation invokes the gray body assumption.

Combining Equations (6) and (7) produces the mathematical expression of our basic model for representing a laboratory spectrum in radiance space:

$$(T_r)_i \propto (\mu_r)_i (\rho_T)_i \,, \tag{8}$$

which we call *Virtual Relative Calibration* (*VRC*). Relation (8) defines a one-dimensional radiance subspace associated with the target. It is a line formed by connecting the point described by the right-hand side of (8) to the shade point. The whitened version is also a line, because the whitening transformation (Equation (2)) is linear.

We remark that although our arguments refer to SWIR data, a claim analogous to relation (8) has been made for visible wavelengths as well, but with a differently formulated mean radiance estimate μ_r (derived from the end members of a linear mixing model [1]). Therefore, the following techniques should apply to visible hyperspectral data as well as to SWIR, with the appropriate mean replacement in (8).

A modification we do not explore here, but which may prove necessary for non-SWIR imagery, concerns the lack of a haze term in Equation (6). Adding a constant, unknown offset term to it, to represent a uniform but unknown path radiance, would convert the one-dimensional target subspace used here into a two-dimensional space and would ultimately produce a different set of detection algorithms. However, their derivations are straightforward extensions of the methods discussed in the next Section.

4. DETECTION ALGORITHMS

4.1. The Affine Matched Filter

If the target/clutter probability functions in Equation (4), (5) contain unknown parameters c and t, then the GLR statistic

$$d(x) \equiv \ln\left(\frac{\underset{t}{Max}\ p_T(x)}{\underset{c}{Max}\ p_C(x)}\right) \tag{9}$$

can be used as a detection algorithm. For example, suppose the clutter parameters c are known from Equation (1). If the t in Equation (9) represents the mean value T of Equation (5) and is treated as a completely unknown vector, then $d(x)$ becomes a standard anomaly detector called RX.

If, on the other hand, the proportionality constraint represented by VRC is imposed, then the only adjustable parameter in the GLR of (9) is the proportionality factor. Condition (8) fixes the direction of T_r, which in turn determines a direction in the whitened space, through the definition $T = C_r^{-\frac{1}{2}} T_r$. Equation (9) then dictates that the amplitude of T be selected to maximize the numerator, that is, to minimize the length of $(x - T)$ (see Equation (5)).

The choice of T that does this cancels the component of x parallel to the T direction. Using this with Equations (4), (5), (8) and (9) produces a detector based on our one-dimensional affine subspace model of the target. It is the affine version of the matched filter:

$$\begin{aligned} AMF(x) &= (x-\mu)^2 - x^t\left(I - \frac{TT^t}{T^2}\right)x \\ &= \frac{(x\cdot T)^2}{T^2} - 2\mu\cdot x + \mu^2. \end{aligned} \tag{10}$$

(Note that TT^t/T^2 projects any vector into the T direction.) AMF has a simple geometrical interpretation in the whitened space. It first computes the squared Euclidean distance of a test pixel x from the clutter mean, and then compares this to the squared distance of x to the target subspace.

Four illustrative decision boundaries for AMF are plotted in Figure 1. These are slices in the T, μ plane through the D – 1 dimensional level surfaces of Equation (10), corresponding to different detection thresholds. Notice that the bottom form in Equation (10) shows that $AMF(x)$ is independent of any component of x outside the T, μ plane. Therefore, the decision boundaries in Figure 4 are cross-sections of D-dimensional cylindrical surfaces.

4.2. Joint Affine Matched Filter

As reported in references [2, 3], AMF performed well when applied to hyperspectral data derived from NRL's MX20-SW [5] sensor. The output of Equation (10) was many times higher for target pixels than for any background pixel. It was noticed, however, that the non-target AMF response was largest for dark pixels. As depicted in Figure 1, they lie far from the bulk of the clutter and close to the target subspace. These could be problematical for more difficult targets. Therefore, a second detection algorithm was conceived to address the dark pixel problem.

This Joint AMF (*JAMF*) invokes a model with a clutter subspace, in addition to the basic AMF target subspace. JAMF is designed to capture the advantages of AMF while mitigating the effects of dark pixels. It does this by extending the core clutter model of (4) to allow for darkened versions of the pixels that generated the core clutter statistics. This is achieved by replacing the clutter mean in Equations (4) and (9) by a vector in the same direction, but with unknown amplitude.

This requires a second maximization operation (in the denominator of (9)), but this is the same mathematical problem solved in the AMF derivation. The net effect is to replace the clutter term in (10) with a projection term, resulting in

$$JAMF(x) = x^t\left(I - \frac{\mu\mu^t}{\mu^2}\right)x - x^t\left(I - \frac{TT^t}{T^2}\right)x = \frac{(x\cdot T)^2}{T^2} - \frac{(x\cdot\mu)^2}{\mu^2}. \quad (11)$$

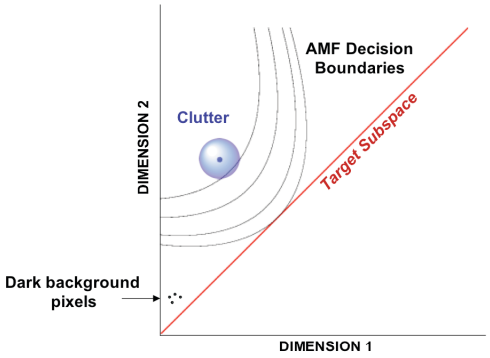

Figure 1. AMF decision boundaries (for four choices of threshold setting) separate the regions where pixels are declared either target (to the right and below) or clutter. All components orthogonal to the plane are ignored.

The latter form shows that, like AMF, JAMF operates on only the projection of any test pixel x into the T, μ plane. In test data, this algorithm substantially reduced the signals originating in dark pixels, as documented in [2, 3]. Figure 2 should be contrasted with Figure 1, to see how the JAMF decision regions can succeed in rejecting dark pixels, because they are near the clutter subspace.

6. SUMMARY

Theoretical foundations have been established for two detection algorithms that had been derived previously by heuristic arguments only. The Affine Matched Filter is meant to supplant the standard Matched Filter, if some method (such as VCR) is available for generating not a mean target estimate, but a spectral subspace that all targets are expected to be near. AMF also applies, for example, to target signatures that can appear with an unknown level of (uniform) illumination.

The second algorithm, the Joint Affine Matched Filter, was derived by extending the AMF target subspace model to include a clutter subspace, in order to account for the possible appearance of low-reflectance or shadowed pixels.

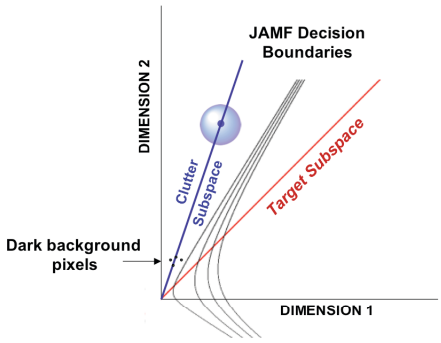

Figure 2. JAMF at 4 threshold settings, which can be chosen to classify dark pixels correctly.

The fact that AMF and JAMF can both be derived from first principles of detection theory is reassuring. One can expect that the simple physical models invoked—of signature uncertainty and dark pixels—can be used to interpret the performance of these and other algorithms on future data sets.

11. REFERENCES

[1] L. S. Bernstein et al., A new method of atmospheric correction and aerosol property retrieval for VIS-SWIR multi- and hyperspectral sensors: QUAC (Quick Atmospheric Correction), Proc. 2004 AVIRIS Workshop, JPL.

[2] A. Schaum, Richard Priest, The Affine Matched Filter, accepted in Proc. SPIE Defense and Security Symposium, 2009.

[3] A. Schaum, R. Priest, The Affine Matched Filter, Proc. Military Sensing Symposium, Las Vegas, NV, Feb. 2008.

[4] Jia Guorui; Zhao Huijie; Li Na, "Simulation of Hyperspectral Scene with Full Adjacency Effect," *Geo-science and Remote Sensing Symposium, 2008. IGARSS 2008. IEEE International* , vol.3, no., pp.III -724-III -727, 7-11 July 2008.

[5] J. Neumann, et al., Demonstration of the MX-20SW Standoff SWIR Hyperspectral Imaging Ball Gimbal System, Proc. Military Sensing Symposium, Las Vegas, NV, Feb. 2008.